scientific reports

OPEN

High sulphur oil of Type II kerogen of the oil shales from Western Central Jordan based on molecular structure and kinetics

Mohammed Hail Hakimi[1,2]✉, Mohammad Alqudah[3], Khairul Azlan Mustapha[4], Ali Y. Kahal[5], Mahdi Ali Lathbl[6], Afikah Rahim[7], Mikhail A. Varfolomeev[2], Danis K. Nurgaliev[8], Ameen A. Al-Muntaser[2] & Shadi A. Saeed[2]

Organic rich sedimentary rocks of the Late Cretaceous Muwaqqar Formation from the Lajjun outcrop in the Lajjun Sub-basin, Western Central Jordan were geochemically analyzed. This study integrates kerogen microscopy of the isolated kerogen from 10 oil shale samples with a new finding from unconventional geochemical methods [i.e., ultimate elemental (CHNS), fourier transform infrared spectroscopy and pyrolysis–gas chromatography (Py–GC)] to decipher the molecular structure of the analyzed isolated kerogen fraction and evaluate the kerogen composition and characteristics. The optical kerogen microscopy shows that the isolated kerogen from the studied oil shales is originated from marine assemblages [i.e., algae, bituminite and fluorescence amorphous organic matter] with minor amounts of plant origin organic matter (i.e., spores). This finding suggests that the studied kerogen is hydrogen-rich kerogen, and has the potential to generate high paraffinic oil with low wax content. The dominance of such hydrogen-rich kerogen (mainly Type II) was confirmed from the multi-geochemical ratios, including high hydrogen/carbon atomic of more than 1.30 and high A-factor of more than 0.60. This claim agrees with the molecular structure of the kerogen derived from Py–GC results, which suggest that the studied kerogen is mainly Type II-S kerogen exhibiting the possibility of producing high sulphur oils during earlier stages of diagenesis, according to bulk kinetic modeling. The kinetic models of the isolated kerogen fraction suggest that the kerogen conversion, in coincidence with a vitrinite reflectance range of 0.55–0.60%, commenced at considerably lower temperature value ranges between 100 and 106 °C, which have produced oils during the early stage of oil generation. The kinetic models also suggest that the commercial amounts of oil can generate by kerogen conversion of up to 50% during the peak stage of oil window (0.71–0.83%) at relatively low geological temperature values in the range of 122–138 °C. Therefore, further development of the Muwaqqar oil shale successions is highly approved in the shallowly buried stratigraphic succession in the Lajjun Sub-basin, Western Central Jordan.

Kerogen is an important component in the organic-rich sedimentary rocks, and plays a key role in understanding hydrocarbon production. Three types of kerogen (Type I, Type II, and Type III) can be revealed from a Van-Krevelen type diagram depends on hydrogen/carbon (H/C) and oxygen/carbon (O/C) atomic ratios[1,2]. Therefore

[1]Geology Departments, Faculty of Applied Science, Taiz University, 6803 Taiz, Yemen. [2]Department of Petroleum Engineering, Kazan Federal University, Kazan, Russia 420008. [3]Department of Earth and Environmental Sciences, Yarmouk University, Shafeeq Irsheidat Street, Irbid 21163, Jordan. [4]Department of Geology, University of Malaya, 50603 Kuala Lumpur, Malaysia. [5]Geology and Geophysics Department, College of Science, King Saud University, Riyadh, Saudi Arabia. [6]Department of Geoscience, Universiti Teknologi PETRONAS, 32610 Seri Iskandar, Perak, Malaysia. [7]Department of Geotecnics and Transportation, Faculty of Civil Engineering, Universiti Teknologi Malaysia, 81310 Johor Bahru, Malaysia. [8]Institute of Geology and Petroleum Technologies, Kazan Federal University, Kazan, Russia 420008. ✉email: ibnalhakimi@yahoo.com

it has gained significant value since it is an important in conventional and unconventional exploration[3]. However, the oil and gas generated from kerogen are linked to the structure and thermodynamic properties of kerogen[4].

The kerogen, without definition the molecular structure, is a mixture of organic compounds and can generate quantities of hydrocarbons. In this regard, several studies have applied several experimental technologies to investigate the molecular structure and properties of the kerogen[5–14]. Such techniques include X-ray photoelectron spectroscopy (XPS), X-ray absorption near-edge structure (XANES), pyrolysis–gas chromatography–mass spectrometry (Py–GC–MS), fourier transform infrared (FTIR) and ^{13}C nuclear magnetic resonance (^{13}C NMR) spectroscopy. These studies have evaluated the structural features in the kerogens based on the disparity between the aliphatic carbon chains and numbers of carbon in aromatic component during the maturity, and thereby understanding the thermally decomposition of different types of kerogen[6].

The key focus of the present study is the oil shales in Jordan, which is distributed in the north, central and south, with reserve reaching to 64.9 billion ton[15,16]. Despite this, oil shales condense in four well known sub-basins such as Lajjun, Yarmouk, Azraq-Hamza, and Jafr[17]. The oil shale deposits in these Jordan's sub-basins are promising unconventional oil resources contributing into the future energy prospect in Jordan. The Lajjun sub-basin in the Western Central Jordan has the largest and more condense oil shale succession in Jordan[15]. This sub-basin includes Attarat Umm Ghudran, Lajjun, Sultani, and Wadi Maghar areas (Fig. 1A).

The oil shales in Jordan range from the Late Cretaceous to Eocene in age as assigned by Alqudah et al.[17,20], and a description of those strata has been performed by Ali Hussein et al.[21,22]. However, many researchers have reported that the Mesozoic (Late Cretaceous) and Cenozoic (Paleocene) oil shales found within the Lajjun sub-basin in western Central Jordan, and have been investigated those oil shale successions in order to gain insights into their origin, depositional environment, quality, and commercial development[15,17,21,23–26]. These prior studies primarily focused on the geochemical characteristics of the whole rock of these oil shales, and indicate that the oil shales in the Lajjun sub-basin possess both economic and scientific importance for unconventional exploration.

This study aims to provide a perception of the molecular structure and properties of the kerogen components found in the organic-rich shale intervals situated within the Late Cretaceous Muwaqqar Chalk Marl Formation (MCM) at Lajjun outcrop, Western Central Jordan (refer to Fig. 1A). In this case, the study commences several approaches that are based on the effect of multi-atoms with organic sulphur included on the kerogen molecular structure (KMS) and fill the gap of knowledge dealt with the internal structure of sulphur-rich kerogen and the timing of oil generation. This comprehensive assessment is based on integrated findings from kerogen microscopic and unconventional geochemical analyses together with bulk kinetics modeling.
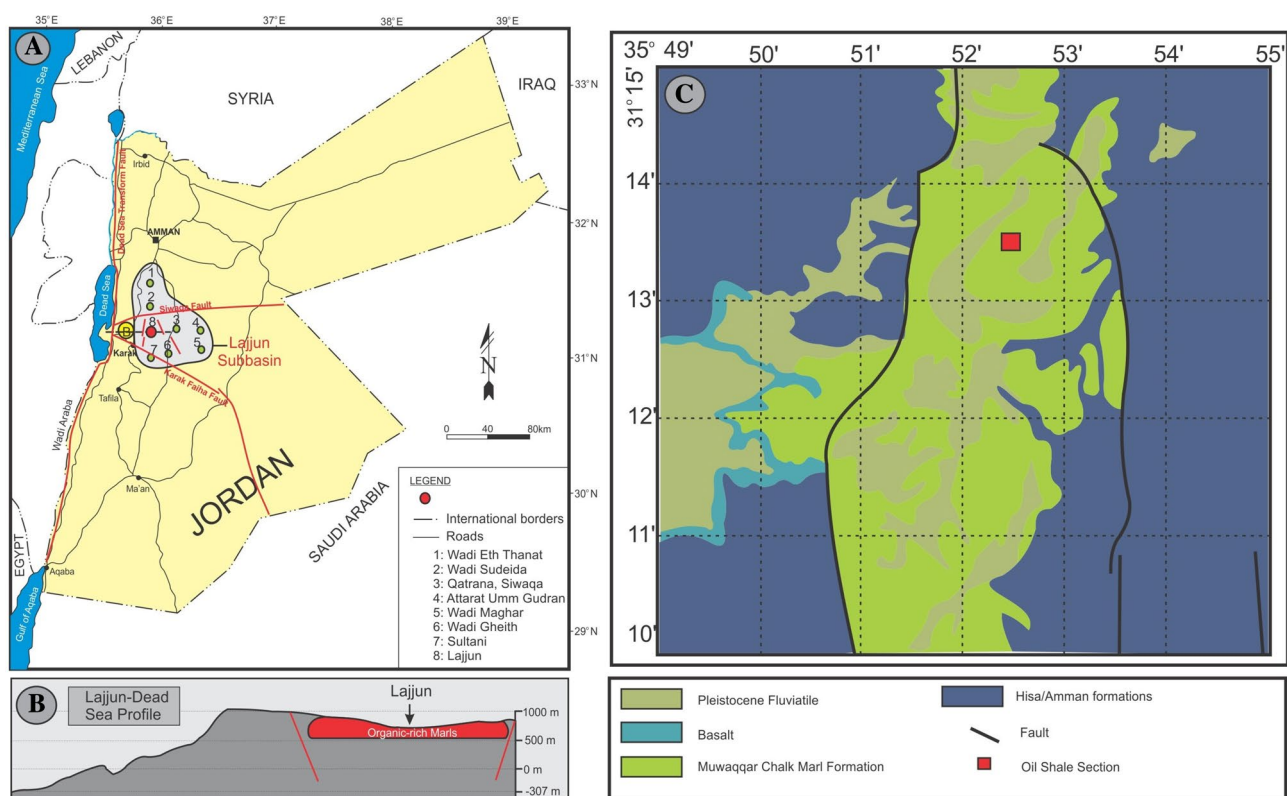
Figure 1. (**A**) Location map of Lajjun sub-basin including 8 major outcrops and related structures (after Ali Hussein[18]). (**B**) Lajjun-Dead Sea cross section showing the main outcrop of the oil shale succession between the two N–S faults (cross section has taken from Google Earth), (**C**) Geological map of the Lajjun sub-basin in Central Jordan, with the main Late Cretaceous Muwaqaar Chalk Marl Formation (modified after Shawabkeh[19]). The maps have drawn by Mohammad Alqudah using Coreldraw15 software.

Geological setting

Jordan was covered with a shallow sea of southern Neo-Tethys Ocean during the Maastrichtian, where organic deposition was initiated in this time[27–29]. Highstand of sea level was influenced during this time, in regional scale with plate tectonics, which thus played a crucial role in formation of morphological features and resulted in a marine transgression over vast areas of the Arabian Plate[17,30,31]. However, the African-Arabian plate initiated a convergence movement toward Eurasia in the Cenomanian left platform deformed into many sub-basins and paleohighs[30,32]. Those sub-basins were characterized with a local restriction which favored for oil shale precipitation between the Middle Cretaceous to Paleogene[33,34].

The biggest sub-basin in the Western Central Jordan is Lajjun sub-basin, which eight outcrops and several subsurface successions were found and described in literatures[26,32,35]. The Lajjun sub-basin encompasses of depression connected by two major faults (Fig. 1B), which is corresponded to the closure of the Neo-Tethys in the Late Cretaceous[36]. Accumulation of sediments in such setting was significantly affected in Lajjun, resulting in increasing in restriction and appearance of organic matter within the sediments of the MCM Formation[22,37]. The MCM Formation is the lithological unit exposed in the Lajjun sub-basin (Fig. 1C), which includes thick bedded marly limestones, marls, chalks, and locally bituminous marls[22,37]. The organic matter of the MCM Formation found in anoxic setting associated with restriction in the sub-basin[22,26,32]. However, those deposits of the MCM Formation seem disconnected and lenticular with a significant variation in thickness over short distances[32], and crop out with few meters thick and around 80 m in the boreholes[37].

In the Lajjun outcrop, the MCM Formation consists of siliceous phosphatic bearing marl at base with strikes of foraminifera (Fig. 2). Organic matter getting more at middle part of the section, which characterize with very dark color (Fig. 2). Limestones in the section are associated with bioturbated intervals. Faunas like gastropods and ostracods are scattered in the samples (Fig. 2).

Samples and analytical techniques

A section, from the Lajjun exposure in the Lajjun Sub-basin, Western Central Jordan, includes ten organic-rich samples of the Late Cretaceous MCM Formation was investigated (Fig. 2). The weathered surfaces of the studied samples were avoided prior to perform the geochemical and petrological analyses. The T_{max} values of the samples are lower than 430 °C according to previous published research[26]. Although T_{max} can be influenced by many non-thermal factors[38], the samples can be generally classified as immature.

The collected whole oil shale samples were milled into ≤ 2 mm, and then employed for used petrographic examination (i.e., organic matter facies). In addiation, the kerogen was isolated from the whole oil shale samples using a palynological procedure of extraction. In this case, the whole samples were crushed into 72 mesh sizes using a mortar and pestle, and then treated to remove the carbonate and silicate minerals using hydrochloric and hydrofluoric acids followed by washing of water to let the sample normalized. The kerogen residuals were sieved and mounted on slides using glycerine jellies. Oxidation and ultrasonic vibration were avoided to get more preserved organic matter. Later, the isolated kerogen was subjected to unconventional geochemical analyses and microscopic examination, including ultimate elemental (CHNS), FTIR analysis, Py–GC, and bulk kinetic modeling together with paleofacies studies. These analyses were performed at geochemical and organic petrological labs in the Department of Geology, University of Malaya, Malaysia.

Microscopic examinations

The whole oil shale samples underwent organic petrological examination and organic facies analysis using a standard polished block procedure[39], as described in the following subsection.

The entire rock volume of the 10 samples was ground into small portions range from 2–3 mm, and then gathered with a SeriFix resin and hardener agent. Then, in order to let surface smoothed, silicon carbide paper and alumina powder were used following ASTM D2797-04. The polished blocks were then examined under white light with oil-immersion medium, cross-polarized and under UV light. LEICA DM4 microscope was used which prepared with fluorescence that allowed a good view of the organic matter (OM) input.

In addition, palynofacies analysis was conducted on the isolated kerogen using traditional thin section under a LEICA DM4 microscope. A total of 200 or more specimens for each sample including (i.e., amorphous organic matter, palynomorph and phytoclasts) were counted using transmitted cross-polarized and UV lights for palynofacies analyses (identifications and quantitative analysis).

Py–GC

Py–GC analysis was employed on the kerogen concentrate after removal of free hydrocarbon (S_1) by Soxhlet extraction procedure and mineral matters by acids leaching procedure (HCL and HF). The Py–GC is useful to identify kerogen types and determine their oil generation potential. Kerogen was heated to 600 °C using a Frontier Lab Pyrolyzer (PY-2020iD), which was connected to an Agilent Technologies 5975 gas chromatograph fitted with an ultra-alloy capillary column (30 m × 0.32 mm I.D. × 0.25 μm) and flame ionisation detector (FID). The major compounds and components were recognized through matching the resultant retention times with standard published samples[40,41].

CHNS

CHNS analysis was performed on the isolated kerogen fraction from 10 oil shale samples using Perkin Elmer (2400 Series II). The isolated kerogen samples were placed into aluminum vials and automatically injected following ASTM standard (P/N 0240–1289). The samples were heated at 1100 °C and then the composition of C, H, N and S were measured. Ascertain additional values, like oxygen content (O %), H/C and O/C atomics were estimated from the combination of elemental compositions (CHNS).
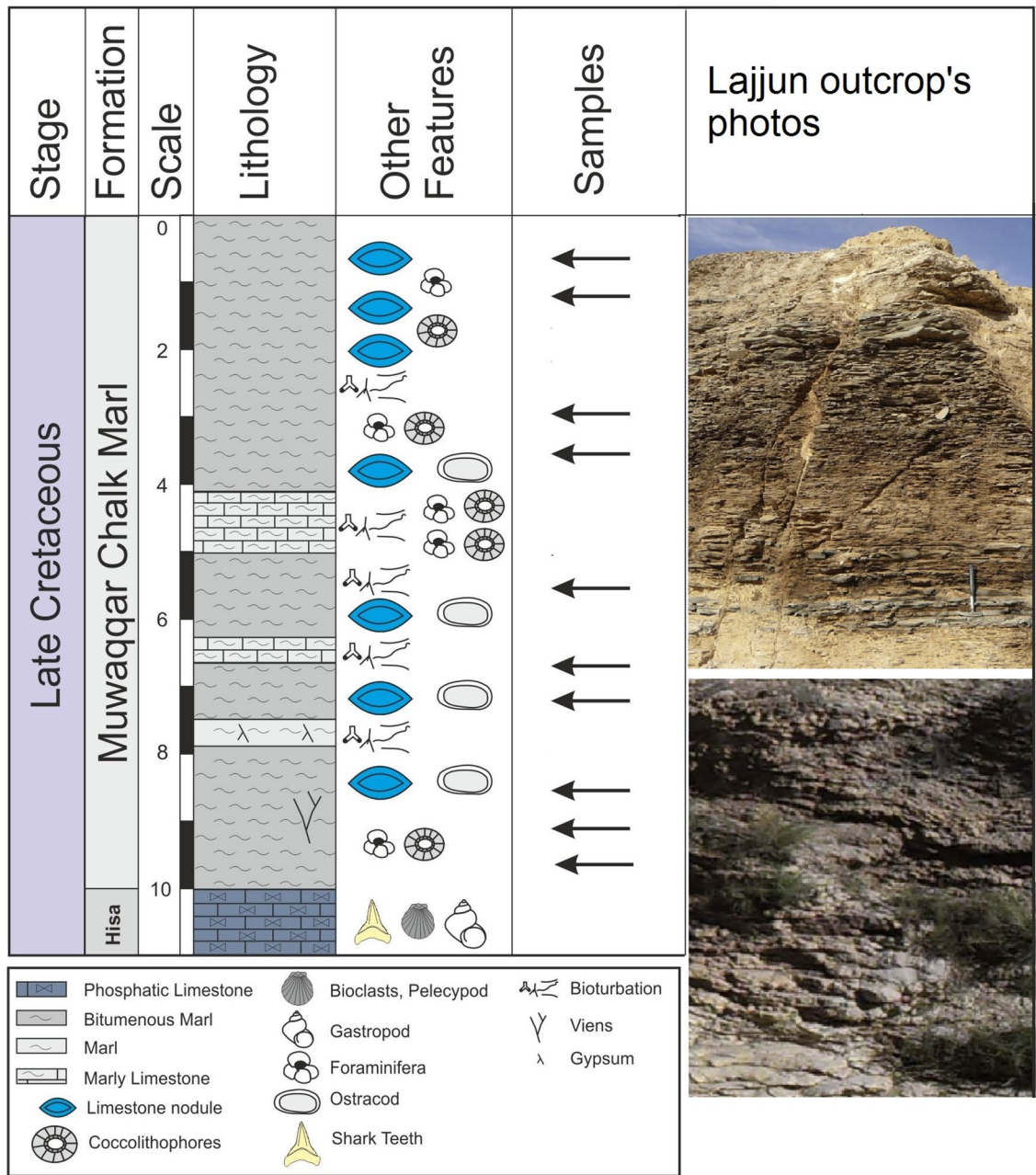
Figure 2. Sedimentological section of the Lajjun outcrop in the Lajjun Sub-basin, Western Central Jordan represents the lithology and the bio-contents in the oil shale samples of Late Cretaceous Muwaqaar Chalk Marl Formation. The section has drawn by Mohammad Alqudah using Coreldraw15 software.

FTIR analysis

ATR-FTIR analysis, which is a commonly used to determine the distribution pattern of varies isolated kerogen groups in the studied organic-rich samples[42,43]. This analysis was performed on a PerkinElmer Spotlight 300 FT-IR microscope system. In this regard, 3 mg of the powdered samples were put on the Diamond/ZnSe plate of the PerkinElmer Universal ATR accessory unit. The infrared spectra were measured in both transmittance and absorbance modes at 4000–650 cm^{-1} wavelength frequency and the peaks were assigned based on published spectra[42–46].

Bulk kinetics modeling

The precipitated kerogen fraction from four oil shale samples was subjected to the bulk kinetic study. These four samples were pyrolyzed using the unstable thermal settings in the Weatherford SRA pyrolyzer under incrementally heating rates starting with 1 at 300 °C and increases to 5, 10, 25 and finalize with 50 °C/min at 600 °C. The results were analyzed using Kinetics 2000 and KMOD software packages and applied to estimate the activation energies (Ea) and the frequency factor (A) following the works of Burnham et al.[47,48] and Behar et al.[49]. Curves

that represent heating rate were considered as essential information to confirm the aforementioned characteristics (Ea and A)[50,51].

Results

Organic matter characteristics

Organofacies in the studied oil shale samples were identified by means of microscopic examination under UV radiation reflected light, as shown in Fig. 3. The organofacies are dominated by high amounts of liptinite, including structured and unstructured organic matter. The liptinites have fluorescence colours fluctuated from orange to yellow (Fig. 3). However, the hydrogen-rich liptinites display a high abundance of the alginate, and they were identified into telalginite and lamalginite based on their morphologies (Fig. 3).

Telalginite arises from algae and appears in many shapes like fan-shaped, discs and lenses (Fig. 3d and e), whereas lamalginite occurs as thick lamellae (Fig. 3a–d).. Other unstructured organic matter such as bituminite also occurred in the studied samples (Fig. 3e and f). The bituminite have a greenish to yellowish fluorescence under UV light (Fig. 3e and f).. Foraminifera assemblages are dominant in the studied samples, which were
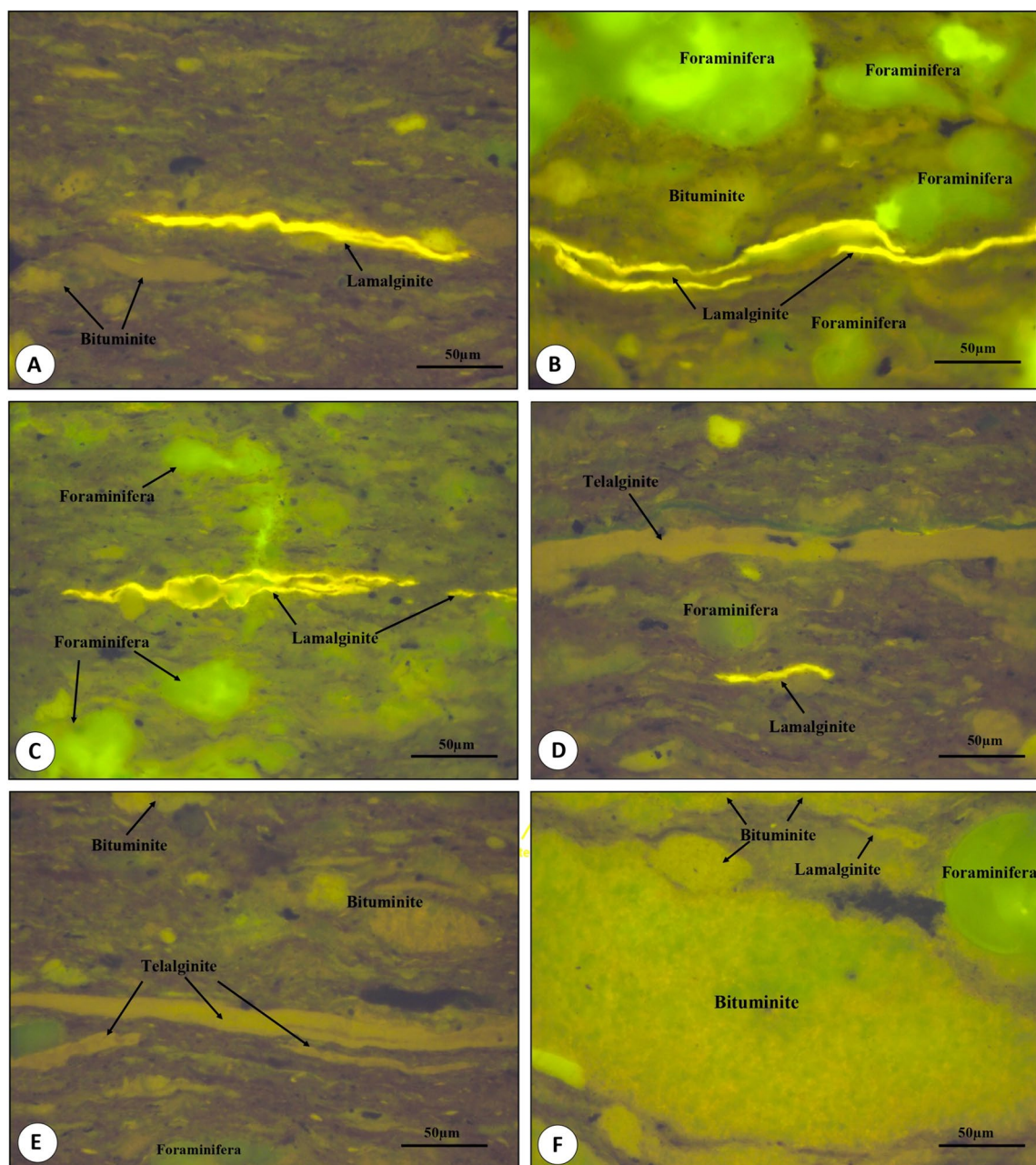
Figure 3. Photomicrographs of the studied oil shales samples of the Muwaqaar Chalk Marl Formation, under reflected UV light, with a field width of 0.2 mm, including different organic matter assemblages of liptinite such as alginite and bituminite.

infused with the mineral matrix and characterized by a greenish fluorescence when examined under the UV light (Fig. 3b,c and f).

Palynofacies and kerogen facies

Based on the palynofacies results, the most predominant component of the kerogen in the studied oil samples was fluoramorphinite amorphous organic matter (AOM) materials, with amount of herbaceous and algal organic matter being fairly low (Fig. 4). The structureless AOM appears to be light to dark brown, well aggregated with angular texture (Fig. 4A–D), while the fluorescence was orange to yellow under UV light (Fig. 4E–H).

Algal organic matter was also found in lower quantities and represent tasmanite (Fig. 4B and F), prasinophyte (Fig. 4C and G), and pediastrum algae types (Fig. 4D and H) based on their morphologies. However, the existence of tasmanite algae pointed that that the studied kerogen fragments contain hydrogen-rich telalginite and lamalginite algae assemblages, as exposed to reflect UV light (Fig. 3). Moreover, the herbaceous organic matter––identifiable species of spore found as minor or absent (Fig. 4B,D,F and H).

Ultimate elemental (CHNS)

The ultimate elemental results show that the carbon contents are relatively high, ranging from 50.61 to 66.99 wt%, while the medium is 63.39 wt%. Hydrogen varies from 6.73 to 8.28 wt%, while nitrogen ranges from 1.25 to 1.93 wt% (Table 1). The sulphur content was also measured and found in high amounts, ranging from 11.18 to 14.19 wt% (Table 1). The oxygen values were estimated based on the CHNS contents and were found to be in the range of 9.05–30.23 wt% (Table 1). Accordingly, the atomic ratios H/C and O/C were obtained with values from 1.46 to 1.60 and from 0.10 to 0.45, respectively (Table 1).

FTIR results

The spectra of representative samples show distinct bands in the aliphatic stretching, aromatic C–H stretching, and aromatic bending regions at 3000–2800 cm^{-1}, 3100–3000 cm^{-1}, and 1460–1350 cm^{-1}, respectively (Fig. 5). Furthermore, methylene (CH_2) groups were recognized based on the appearance of peaks near 2920 cm^{-1} and 2850 cm^{-1}, while the peaks near 1600 cm^{-1} were given an aromatic C=C groups (Fig. 5). The spectra also display the asymmetric CH_3 stretching anomaly at 2955 cm^{-1} and carboxy/carboyl group peak at 1710 cm^{-1}. Based on the spectra of FTIR results, several parameters, including A-factor (AF), C-factor (CF), aliphaticity index (IAL), aromaticity index (IAR) are calculated (See Table 1). The AF is a proportion of the abundance of aliphatic over aromatic bands, while CF is a measure of the relative abundance of carboxyl over carboxyl and aromatic bands. The IAL and IAR, respectively, quantify the relative intensities of aliphatics and aromatics to saturate and aromatics. These FTIR parameters are useful for evaluating hydrocarbon generation potential and classifying kerogen portions, as argued in the coming sections.

Py–GC

Py–GC results show that the isolated kerogen is characterized by unimodal chromatogram patterns of the n-alkene and n-alkane doublets, ranging from C$_{1-5}$ to C$_{30}$ (Fig. 6). The distribution of these n-alkene and n-alkane doublets is characterized by high abundance of low n-alkane molecules (C$_{1-5}$–C$_{14}$), with low quantities of waxy n-alkene and n-alkane (+ C$_{15}$), as shown in Fig. 6. The dominant aromatic compounds observed in studied samples are toluene and o-xylene (Fig. 6). Higher amount of 2,3-dimethylthiophene is also observed laterally with aromatic and saturated hydrocarbons (Fig. 6).

However, the proportions of four components, namely carbon 8,2,3-dimethylthiophene, o-xylene and carbon 9:1 in the pyrolysates of the analyzed isolated kerogen in the studied samples (Fig. 6) were estimated as shown in Table 2. The pyrolysate distributions of these three components show a majorly 2,3-dimethylthiophene compound and C$_8$ n-alkane, along with minor quantities of C$_{9:1}$ n-alkane and o-xylene compound (Fig. 6), leading to a percentage 40.03–53.09%, 16.71–22.13%, 15.55–19.94%, and 14.51–18.30%, respectively (Table 2).

The o-xylene related to C$_8$ n-alkane, showing richness of C$_8$ n-alkane over o-xylene, with values of the o-xylene/C$_8$ and C$_8$/o-xylene proportion from 0.75 to 0.87 and from 1.15 to 1.34, respectively (Table 2). Table 2 also illustrates the relative abundance of the C$_1$-C$_5$, C$_6$-C$_{14}$ and C$_{+15}$ of the n-alkane and n-alkenes that measured from the Py–GC pyrograms of the resulted kerogens. Most of the samples show that the C$_6$–C$_{14}$ of the n-alkane and n-alkenes prevails (41.72–54.18%) over than the C$_1$–C$_5$ (32.15–48.27%) and C$_{+15}$ (10.01–16.92%) of the n-alkane and n-alkenes.

Bulk Kinetic results

The bulk kinetic results of the isolated kerogen fraction from three studied samples are illustrated in Fig. 7. The bulk kinetic models (Fig. 7a) suggest that the Ea patterns are intensively fluctuated from 39 to 66 kcal/mol, while A is found to be between 2.1237E+13/1 and 5.0950E+13/1 s.

The kinetic models at a consistent rate at a 3.3 °C/My rate were also used to estimate the geological heating, thus paleo-temperatures and the therefore the vitrinite reflectance (%Ro) values and transformation ratio (TR) was accordingly predicted. In this case, the paleo-temperatures are plotted against the calculated %Ro and TR values and the results are presented in Fig. 7b, and show that the earlier stage of petroleum generation window (% 10 TR) takes place at 100–106 °C, which matches to a estimated %VRo is between 0.55 and 0.60, while the peak generation window, with corresponding Ro of 0.71–0.83% is expected to convert around 50% of kerogen during the geological temperatures between 122 and 138 °C (Fig. 7b), and thereby can generate significant amounts of oil.
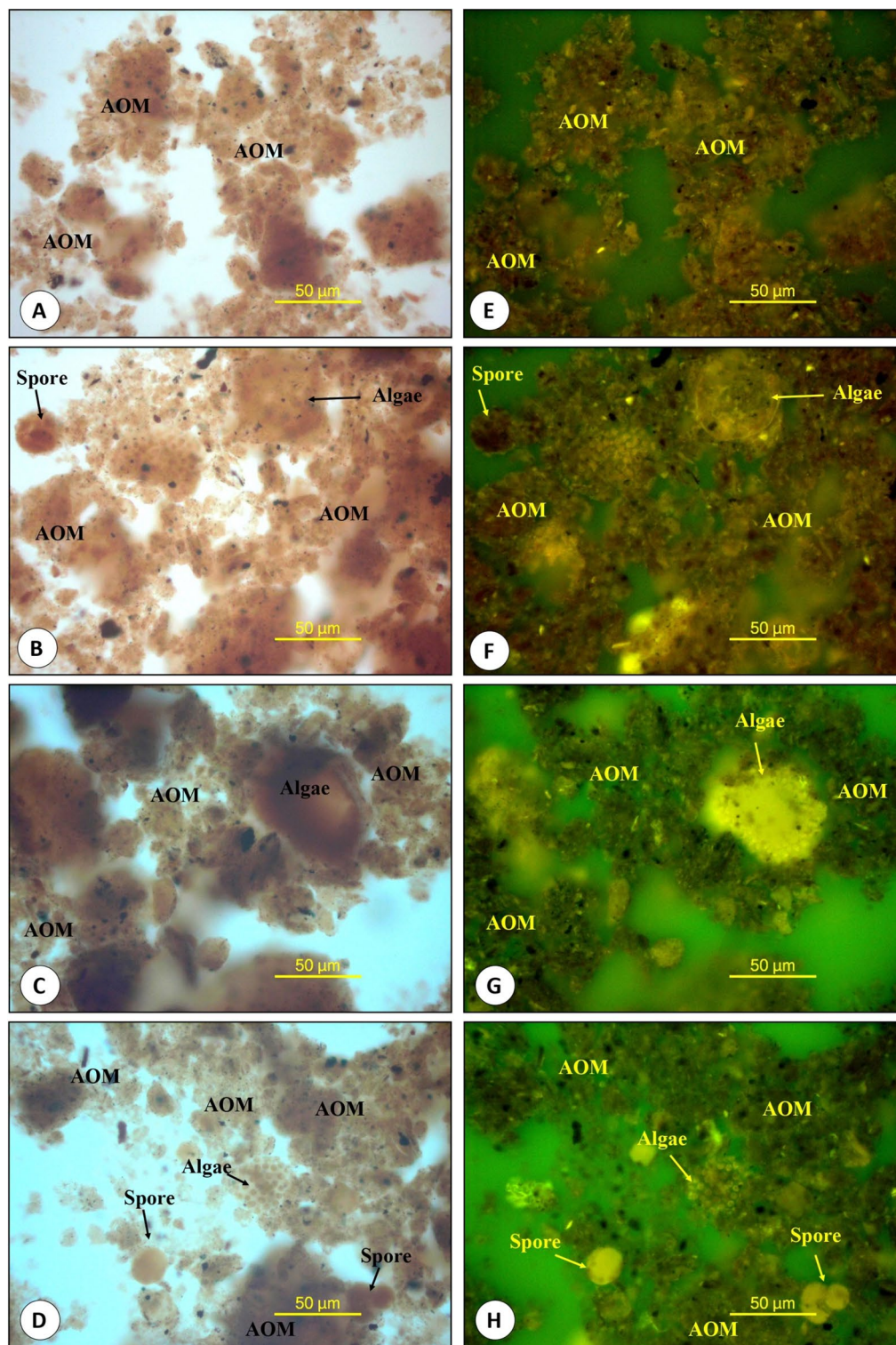
Figure 4. Photomicrographs of the isolated kerogen in the studied oil shales samples of the Muwaqaar Chalk Marl Formation, under transmitted normal (**A–D**), and UV (**E–H**) lights, with a field width of 0.2 mm.

Discussion

Kerogen composition and characteristics

Herein, we discuss the molecular structure of the isolated kerogen fraction together with the visual kerogen properties in order to get insight into the kerogen composition and characteristics from oil shales in the Late Cretacouse succession.

Sample ID	Fourier transform infrared (FTIR) results				Ultimate elemental (CHNSO) analysis									
	AF	CF	IAL	IAR	C wt%	H wt%	N wt%	S wt%	O wt%	C	H	O	Atomic H/C	Atomic O/C
KOS-1	0.65	0.51	0.62	0.40	62.16	7.83	1.49	12.20	16.31	5.18	7.83	1.02	1.51	0.20
KOS-2	0.67	0.51	0.63	0.39	66.29	8.28	1.58	14.05	9.80	5.52	8.28	0.61	1.50	0.11
KOS-3	0.66	0.51	0.63	0.39	50.61	6.73	1.25	11.18	30.23	4.22	6.73	1.89	1.60	0.45
KOS-4	0.66	0.50	0.63	0.39	65.10	7.96	1.62	12.92	12.40	5.42	7.96	0.78	1.47	0.14
KOS-5	0.65	0.50	0.62	0.38	66.85	8.15	1.67	14.19	9.15	5.57	8.15	0.57	1.46	0.10
KOS-6	0.68	0.53	0.64	0.38	66.99	8.19	1.64	14.13	9.05	5.58	8.19	0.57	1.47	0.10
KOS-7	0.67	0.52	0.63	0.38	64.35	8.03	1.57	13.46	12.59	5.36	8.03	0.79	1.50	0.15
KOS-8	0.67	0.51	0.64	0.39	64.17	7.93	1.61	13.59	12.70	5.35	7.93	0.79	1.48	0.15
KOS-9	0.68	0.51	0.63	0.38	64.00	7.85	1.93	13.49	12.72	5.33	7.85	0.79	1.47	0.15
KOS-10	0.67	0.53	0.64	0.37	67.50	7.75	1.40	12.10	25.56	5.63	7.75	1.60	1.38	0.28

Table 1. Ultimate elemental (CHN) and fourier transform infrared (FTIR) results of the isolated kerogen from ten oil shale samples of the Late Cretacouse Muwaqqar Chalk Marl Formation from the Lajjun outcrop in the Lajjun Sub-basin, Western Central Jordan. C, Carbon; H, Hydrogen; O, Oxygen; N, Nitrogen; S, Sulfur, AF, A-factor = [(2930 + 2860) cm^{-1}]/[(2930 + 2860 + 1600) cm^{-1}], CF, C-factor = 1710 cm^{-1}/[(1710 + 1600) cm^{-1}], IAL, aliphaticity index = [(2950 + 2920 + 2850) cm^{-1}]/[(2950 + 2920 + 2850 + 3030 + 1600) cm^{-1}], IAR, aromaticity index = [(3030 + 1600) cm^{-1}]/[(2950 + 2920 + 2850 + 3030 + 1600) cm^{-1}].

The visual kerogen of the studied oil shale samples has a mixture organic facies, with the dominance of marine origin organic matter assemblages (i.e., algae, bituminite and fluorescence AOM) and minor amounts of plant-like fossils (i.e., spores), as clearly indicated from microscopic investigation (Figs. 3 and 4). Most of the algal organic matter in the studied oil shale samples is presented by both telalginite and lamalginite types, which are assumed to have formed in mainly marine environment[26,40,52,53]. Other unstructured organic matter such as bituminite and fluorescence AOM are inferred as bituminite II following Pickel et al.[54] and assigned the origin of the kerogen components to the marine environment[55]. However, these marine organic matter assemblages imply strongly hydrogen-rich kerogen categories. Further, the interpretation of the hydrogen-rich kerogen in the studied oil shale samples is corroborated by the pyrolysates of the kerogen degradation using Py–GC results, which can be used to assess the structural moieties of kerogen that related to alkyl-chain distribution, degree of aromaticity, and thereby gain knowledge on the kerogen types and their petroleum composition[56–62]. In this case, the high abundance of n-alkanes and n-alkanes of more than C_{10} indicates the presence of aliphatic-rich kerogen, while aliphatic-poor kerogen has n-alkanes and n-alkanes of less than C_{10}[62].

In the current study, the analyzed isolated kerogen displays a unimodal distribution pattern of n-alkane and n-alkane doublets, with the prevalence of n-alkane and n-alkane peaks of more than C_{10} and comparatively low aromatic components (Fig. 6). This pyrolysate distribution is further suggested that the analyzed isolated kerogen from the studied oil shale samples was mainly derived from aliphatic-rich kerogen.

Additionally, many literatures have shown that the length and type of aliphatic chains in FTIR spectra and its structure can be used to get information about the kerogen types[42–44,63]. In this regard, the FTIR spectra, particularly aliphatic and aromatic C–H stretching, shows that the analyzed kerogen fraction mainly composed of aliphatic stretching bending regions between 2800 and 3100 cm^{-1}, with lesser amounts of aromatic bending regions at 1460–1350 cm^{-1} (Fig. 5), and confirms the strong aliphatic-rich kerogen. The FTIR spectra-based parameters such as AF and CF have also been used to evaluate the kerogen type[44]. Based on the AF and CF results, the analyzed isolated kerogen fraction has relatively high AF values of more than 0.60 and up to 0.68 (Table 1), suggesting the dominance of mainly kerogen type II, as clearly demonstrated from a modified correlation diagram of AF and CF parameters by provided Ganz and Kalkreuth[44], as shown in Fig. 8a. Moreover, the ultimate elemental analysis of the isolated kerogens is in compatibility together with the molecular structure of the kerogen using FTIR spectra and used to corroborate the organic matter inputs and their kerogen types[64,65]. The higher H/C percentage suggested oil-prone Types I and II kerogen with higher hydrogen content, whereas higher ratios of O/C referred to Type III kerogen that fall within gas-prone[52]. Based on the results, the analyzed isolated kerogen fraction has high H/C values between 1.46 and 1.60 (Table 1), further indicating mainly Type II kerogen, as clearly confirmed from a Van-Krevelen type diagram based on applying the H/C and O/C atomic ratios (Fig. 8b).

The presence of the high S content of > 10 wt% with the molecular structure of analyzed kerogen from the studied Late Cretacouse oil shales usually indicates a high sulphur Type II kerogen[26,66]. This interpretation agrees with the good correlation between the S and H elements (Fig. 9). In addiation, the Type II kerogen enriched with sulphur also was confirmed from the pyrolysates of the kerogen degradation. In this case, the pyrolysate distributions show a majorly 2,3-dimethylthiophene organic sulphur compound, along with minor amounts of $C_{9:1}$ n-alkane and n-alkane doublets and o-xylene compound (Fig. 6), further indicating Type II kerogen enriched in sulpher based on the plot illustrated by Eglinton et al.[59], as shown in Fig. 10.

However, the Ea and A values also infer to the kerogen composition, as they are significantly influenced by the constancies in temperature and thermal conductivity of each kerogen group[49,67–70]. Types I and II oil-kerogen exhibit constricted value of Ea covered 47–56 kcal/mol[69,71], the Type II-S kerogen in the other way display a more fixable range of Ea fluctuated between 44 and 66 kcal/mol[26,49,72]. In this regard, the broad activation energy
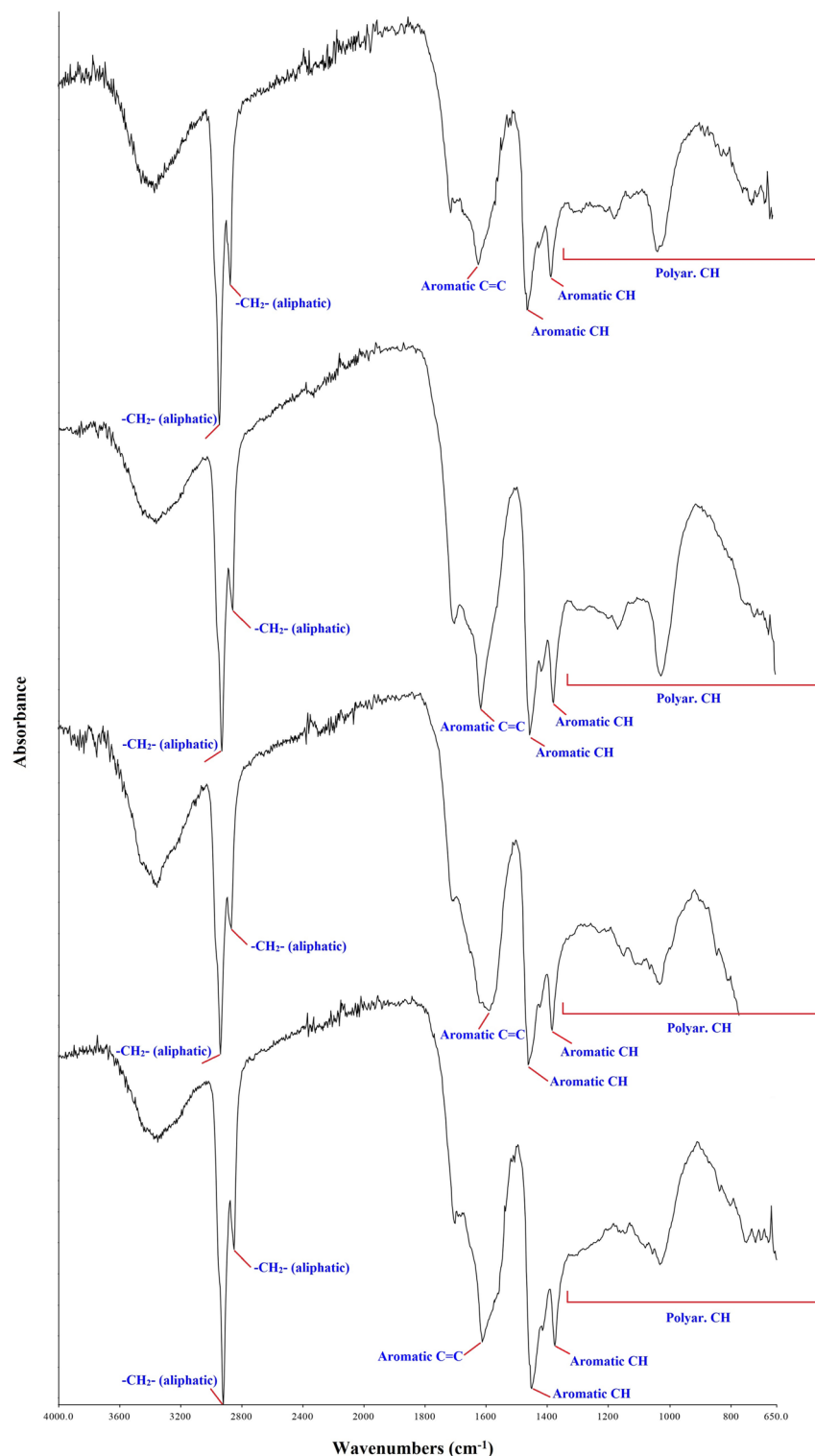
Figure 5. FTIR spectra of the isolated kerogen from representative oil shale samples from the Lajjun outcrop in the Lajjun Sub-basin.

distributions, with an average frequency factor of 3.56E+13/1 s observed in the analyzed isolated kerogen fraction from the studied oil shales are typical for Type II-S kerogen[73].

Implication for unconventional oil shale exploration

In the current study, we considered a variety of parameters to get ideal for the efficacy of the oil production from kerogen within the oil samples of the Late Cretacouse MCM Formation from the Lajjun outcrop, Lajjun Sub-basin
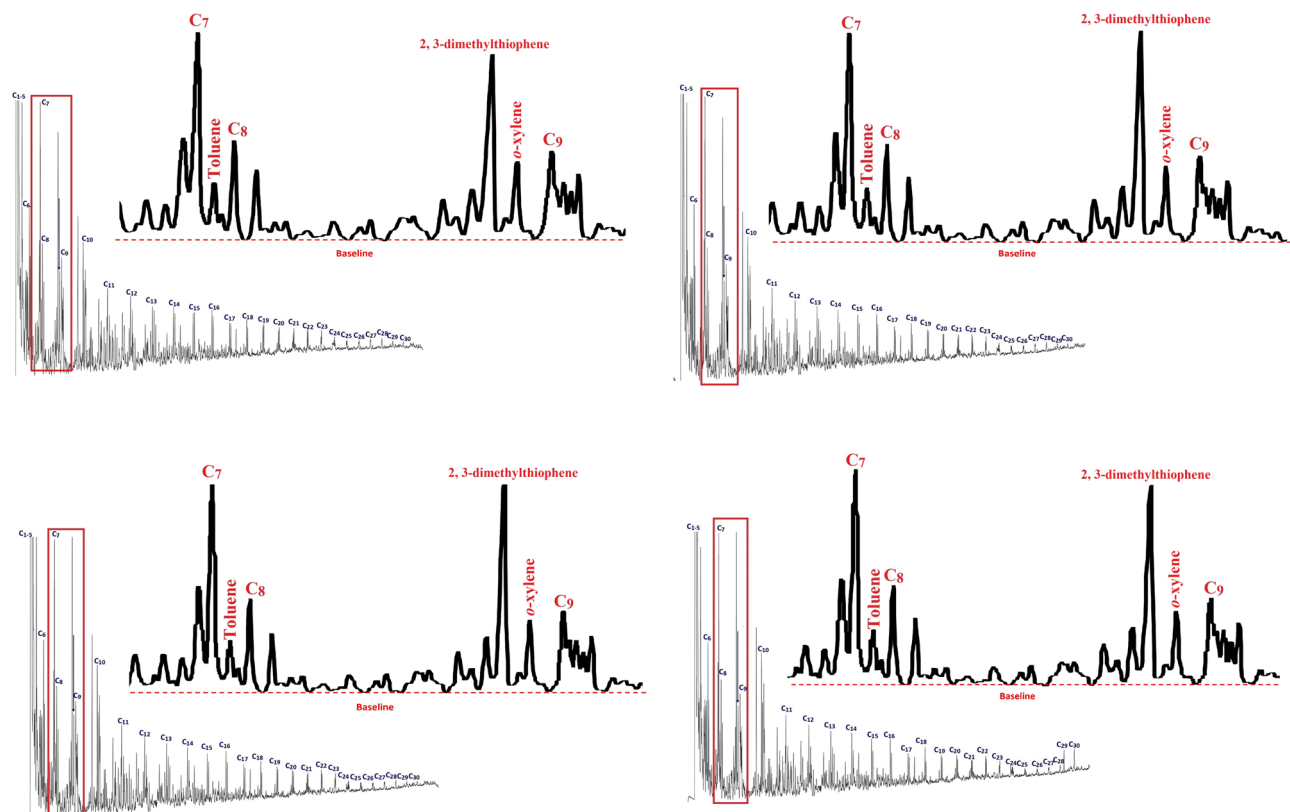
Figure 6. Py–GC pyrograms of the isolated kerogen in the studied oil shales samples of the Muwaqaar Chalk Marl Formation, showing *n*-alkene/alkane doublets and labelled peaks.

| Samples ID | Pyrolysis–gas chromatography (Py–GC) | | | | | | | | |
	2,3-dimethylthiophene (%)	*n*-C$_{9:1}$ (%)	*o*-xylene (%)	*n*-C$_8$ (%)	C$_1$–C$_5$ (%)	C$_6$-C$_{14}$ (%)	C$_{15}$ + (%)	xy/C$_8$ ratio	C$_8$/xy ratio
KOS-1	40.87	19.56	17.44	22.13	38.51	45.42	16.07	0.79	1.27
KOS-2	45.29	18.17	15.91	20.64	40.85	44.52	14.64	0.77	1.30
KOS-3	46.28	17.74	15.59	20.39	40.96	45.48	13.56	0.76	1.31
KOS-4	43.75	18.99	15.91	21.35	32.15	54.18	13.67	0.75	1.34
KOS-5	53.04	15.74	14.51	16.71	48.27	41.72	10.01	0.87	1.15
KOS-6	45.76	18.14	16.06	20.04	41.85	46.02	12.13	0.80	1.25
KOS-7	45.14	18.33	15.89	20.63	40.98	43.99	14.99	0.77	1.30
KOS-8	43.15	19.15	16.12	21.58	37.65	45.43	16.92	0.75	1.34
KOS-9	40.03	19.94	18.30	21.73	40.56	45.56	13.88	0.84	1.19
KOS-10	53.09	15.55	14.55	16.81	40.75	44.34	14.91	0.87	1.16

Table 2. Pyrolysis–gas chromatography (Py–GC) of the isolated kerogen from ten oil shale samples of the Late Cretacouse Muwaqqar Chalk Marl Formation from the Lajjun outcrop in the Lajjun Sub-basin, Western Central Jordan.

of western central Jordan.In this case, multi-geochemical results were discussed based on the molecular chemical structure and visual properties of kerogen and show that the kerogen of the MCM samples is rich in hydrogen and is considered as an oil-rich resource. This finding of the high concentration of hydrogen is evidenced by the ultimate elemental analysis, with dominantly Type II kerogen (Fig. 8b). The notably intensive fluorescent found in the liptinitic organic matter under UV light (Fig. 3 and Fig. 4e,f,g and f) serves as evidence that the studied shale rocks of the MCM succession have the extremely oil generative potential.

The higher quantities of aliphatic carbon chains than aromatic carbon number in the molecular structure of the kerogen is also confirmed by the applied Py–GC and FTIR results (Figs. 5 and 6). Accordingly, the kerogen in the studied MCM samples is mainly Type II kerogen (Fig. 8). The Type II kerogen in the studied samples would have a high sulphur-rich Type II kerogen, as indicated by the essential chemical properties of kerogen, with a high amount of sulphur content exceeds 11 wt% and up to 14.19 wt% (Table 1). II S. However, the highest

(A) activation energy [Ea] distribution and frequency factor [A]

(B) Computed transformation ration [TR%] and vitrinite reflectance [%Ro]
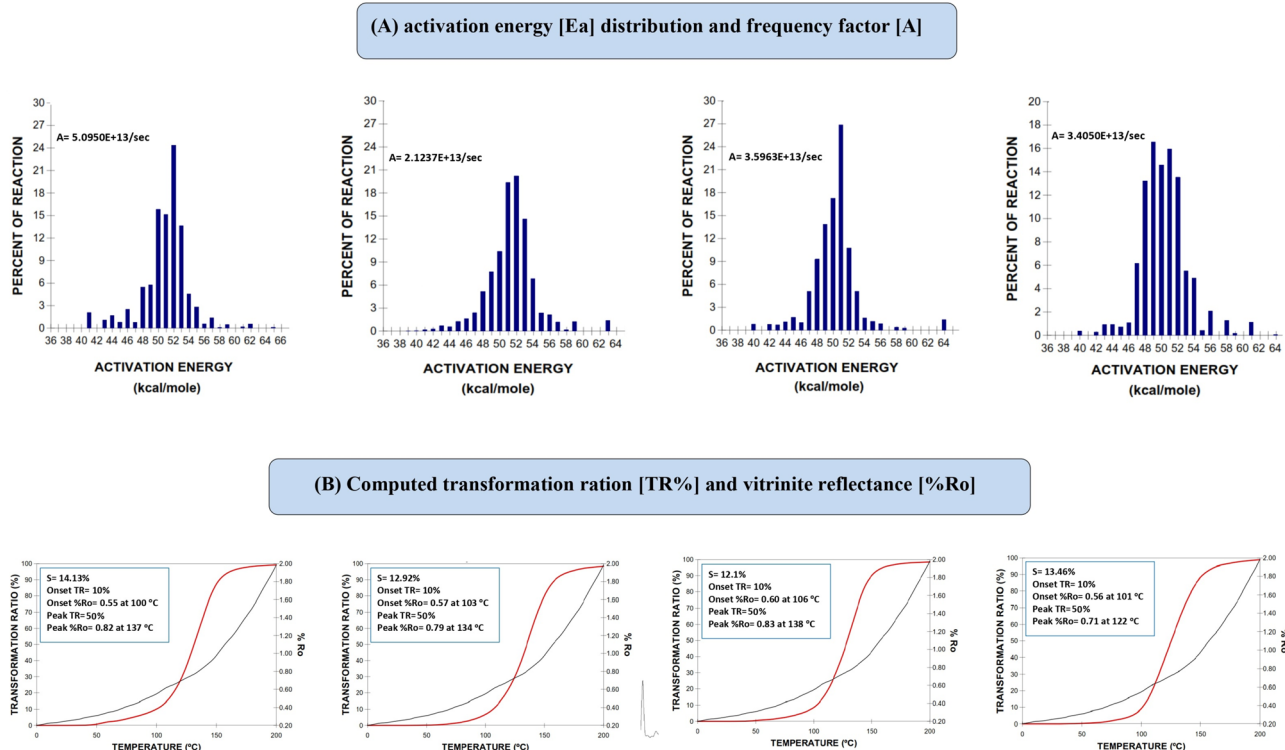
Figure 7. (**A**) Bulk kinetic parameters in terms of activation energy distribution (Ea) and frequency factors (**A**) of the 4 selected kerogen-extracted oil shale samples. (**B**) Bulk kinetic results in terms of temperature (°C), transformation ratio (TR%) and Vitrinite reflectance (Ro%) of the 4 selected kerogen-extracted oil shale samples. Data were determined from open system pyrolysis at five heating rates (1, 5, 10, 25 and 50 °C/min).
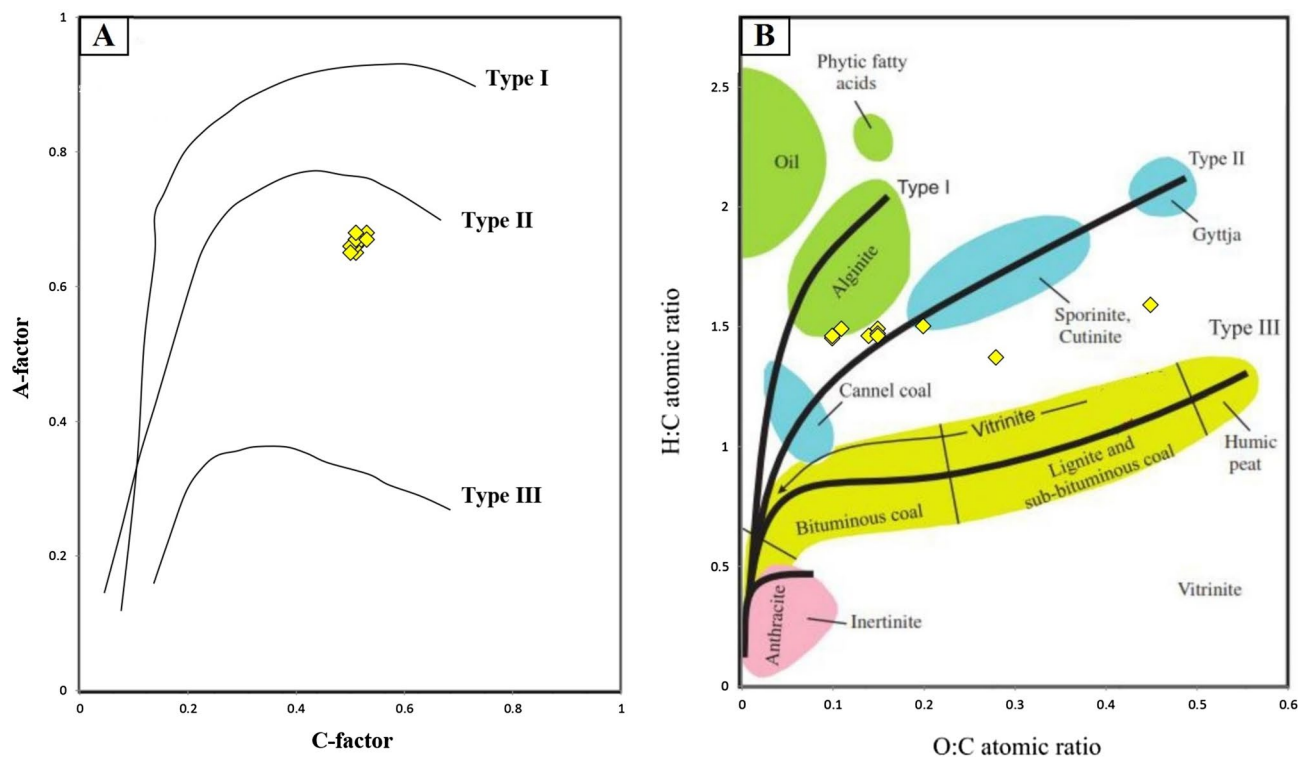
Figure 8. (**A**) Cross plot of the A-factor and C-factor of the FTIR specta for the isolated kerogen of the studied oil shale samples. (**B**) Cross plot of the H/C and O/C atomic ratios of the isolated kerogen of the studied oil shale samples, showing mainly Type II kerogen.
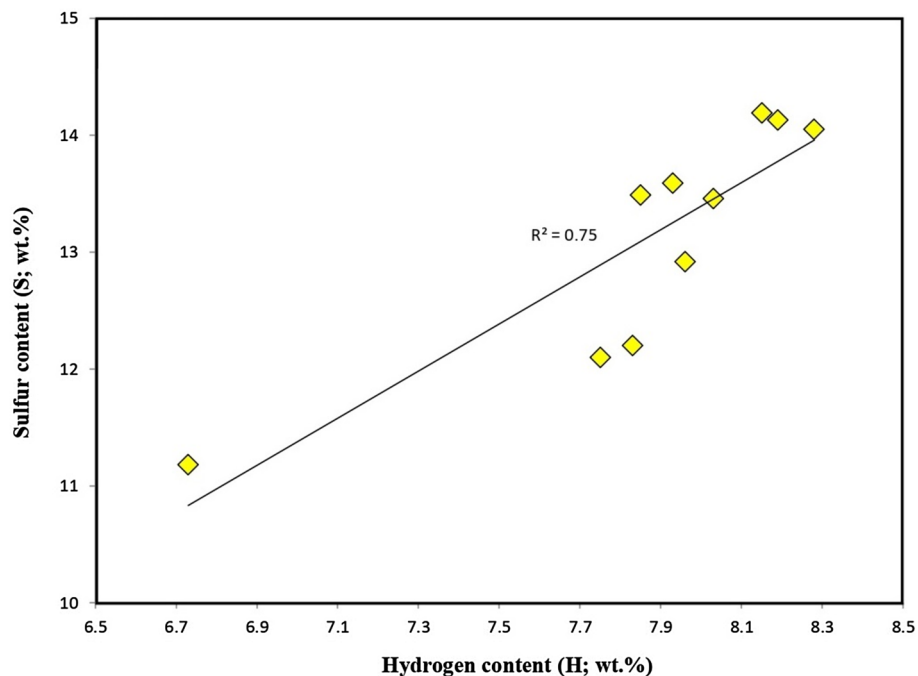
Figure 9. Cross plot of the sulphur (S) content versus hydrogen (H) content of the isolated kerogen in the studied oil shale samples.
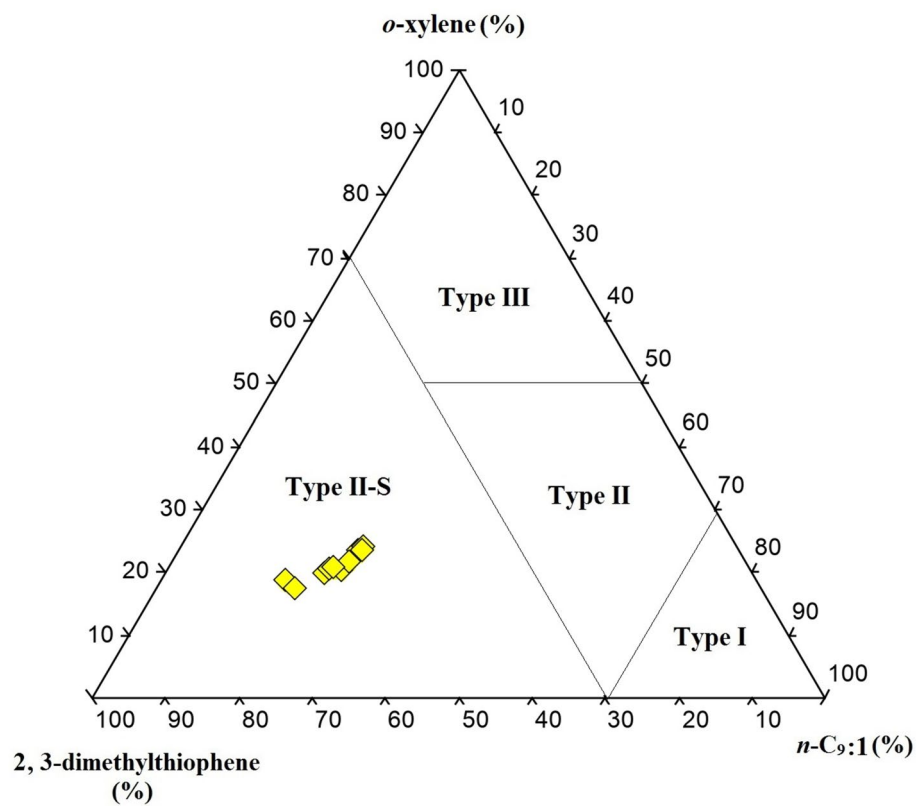
Figure 10. Ternary diagram based on n-alkyl chain length distribution of the pyrolysis products of the analyzed isolated kerogen of the studied oil shale samples (adapted after Eglinton et al.[57]).

organic sulphur, resulting in a mainly sulphur-rich Type II kerogen, as clearly demonstrated by the presence of the high concentrations of sulphur compound (i.e., 2,3-dimethylthiophene) associated with saturated and aromatic hydrocarbons (Fig. 10). In this case, the high sulphur oil can generate from the organic rich sediments of the Late Cretacouse MCM Formation during the early thermal retorting or pyrolysis process. This oil is classified as paraffinic with low wax products (Fig. 11) Besides, petroleum production stages and their geological temperatures of the studied.

In addiation, finding of sulphur in the molecular structure of the kerogen in the Muwaqqar Chalk Marl oil shales enhanced generation of oil over low maturity level stage[72], corresponds to VRo values range between 0.4 and 0.8%[74]. This interpretation is further assessed using bulk kinetics modeling at heat rate of 3.3 °C/My. According to the kinetic models, the kerogen of most of the studied MCM oil shales found to be able to generate oil in the low temperatures (100–106 °C), which was associate with low VRo covered 0.55–0.60 Ro% (Fig. 7b). This is can be explained by existence of a weak bonds between carbon and sulfur (C–S) in the kerogen structure[72], as works with the presence of Type II-S kerogen in the studied oil shale samples of the MCM Formation (Fig. 10). This is clearly demonstrated by the inversely proportional between the high S content and low geological temperature ranges and their equivalent VR values from the kinetic models (Fig. 12).

Furthermore, the kinetic model outcomes of this research works also indicate that the investigated oil shale intervals of the MCM Formation reached the high kerogen conversion ratio of up to 50% during the temperature ranges between 122 and 138 °C, matching to VR values of 0.71–0.83% (Fig. 7b). Therefore, commercial amounts of high sulphur oil can generate at shallow stratigraphic sections in the Lajjun sub-basin, Western Central Jordan. However, the same paleoenvironmental condition found throughout Lajjun sub-basin suggested equivalency of kerogen structure throughout the Lajjun sub-basin[32,35,37]. As one goes through the Lajjun sub-basin, the Muwaqqar Chalk Marl Formation reached few meters thick in the outcrop parts and burial depths between 117 and 150 m, with 25–60 m thick in the boreholes[35]. This indicates that the organic rich sedimentary rocks intervals of the MCM Formation in different portions likely achieved low level of maturity due to the shallow burial temperatures, and can be potential for future development in the retorting of such deposits to extract considerable quantities of sulfur-rich oil using different heating methods such as hydrothermal.

Conclusions

Comprehensive unconventional geochemical methods together with kerogen microscopy of the isolated kerogen from ten oil shale samples of the Late Cretaceous Muwaqqar (MCM) Formation taken from the Lajjun outcrop in the Lajjun Sub-basin, Western Central Jordan were conducted. The following significant inferences were drawn concerning the molecular structure, composition and characteristics of the kerogen and implications on its potential for unconventional oil exploration. The results are drawn the following major conclusion:
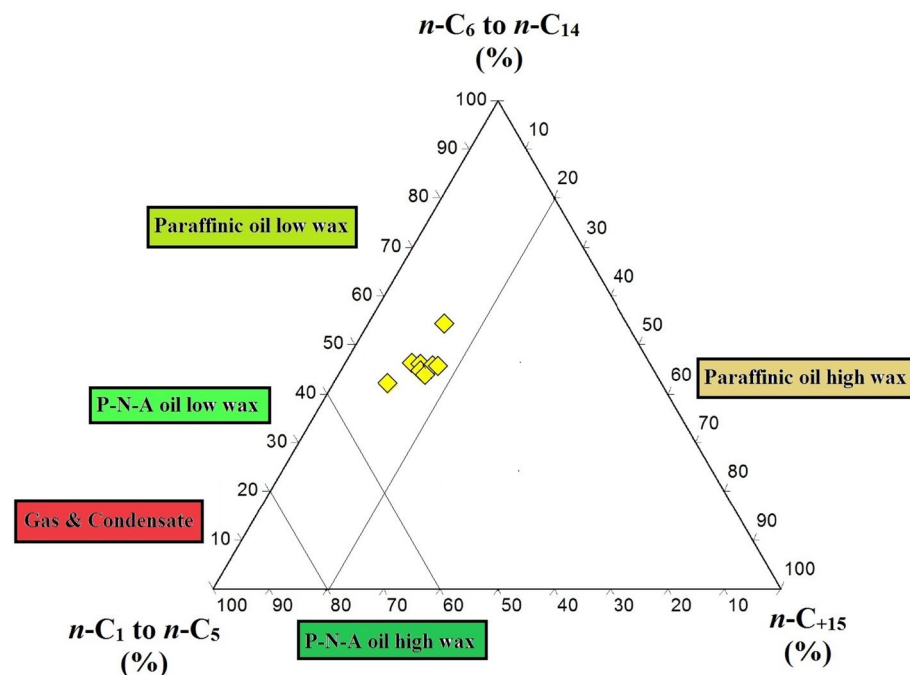
Figure 11. Ternary diagram based the relative percentages of the *n*-alkenes/*n*-alkane ranges, shown the oil types that can generate during decompacting or pyrolysis processes of the analyzed isolated kerogen in the studied oil shale samples (modified after Horsfield[72] and Yang et al.[41]).
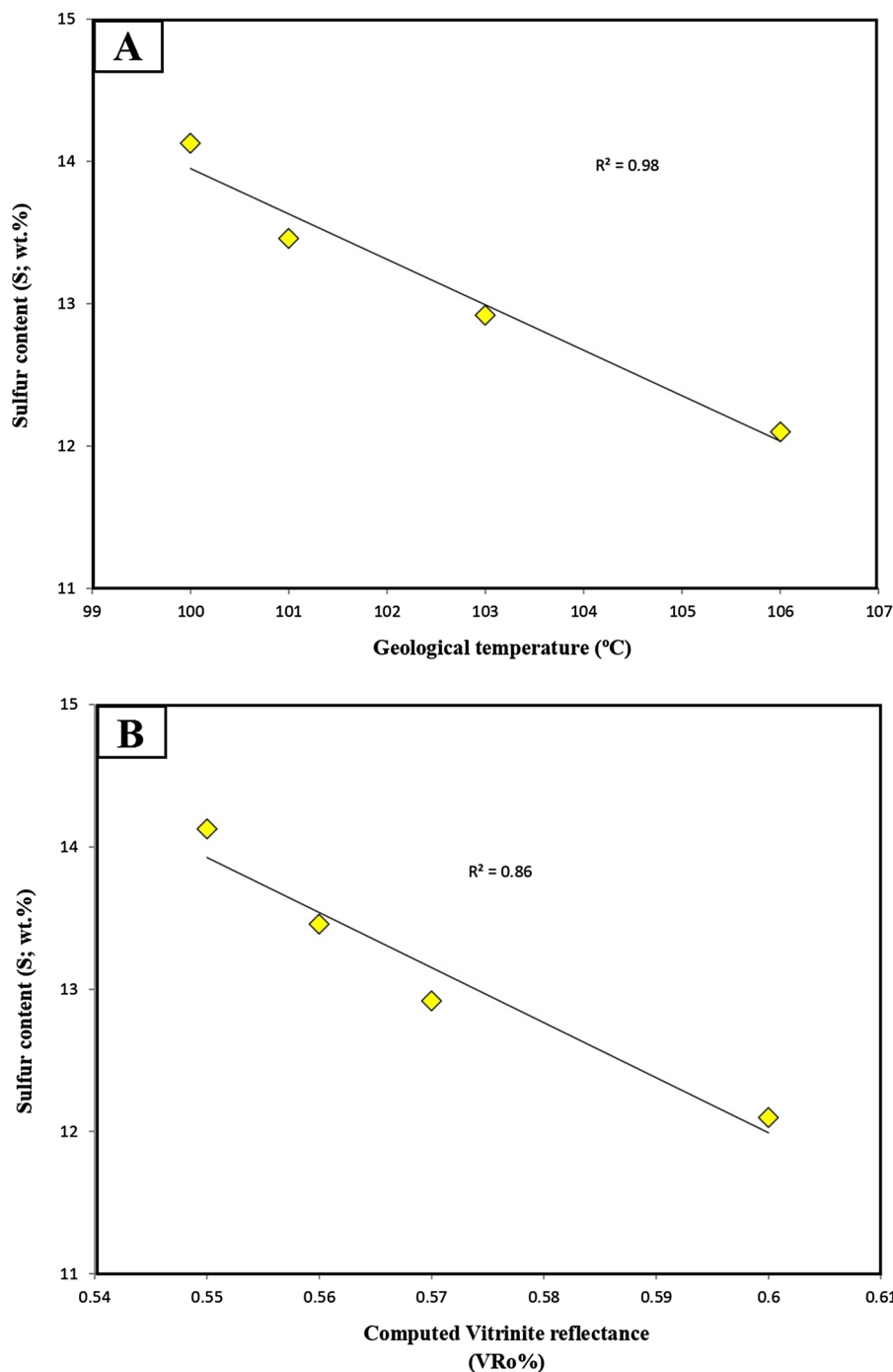
Figure 12. (**A**) Cross plot of the sulphur (S) content versus hydrogen (H) content of the isolated kerogen of the studied oil shale samples. (**B**) Cross plot of the sulphur (S) content versus carbon (C) content of the isolated kerogen of the studied oil shale samples, showing the inverse proportional between the high S content and low geological temperature ranges and their equivalent VR values from the kinetic models.

1- The studied oil shale samples contain high abundance of reactive liptinites, mainly algae and fluorescence AOM with minor amounts of spore, indicating kerogen enriched in hydrogen for strong oil generation potential.

2- According to ultimate elemental and FTIR results, the isolated kerogen from the studied oil shale samples is mainly Type II kerogen, with high hydrogen/carbon atomic ratio of more than 1.30 and higher A-factor of aliphatic stretching CH_2 than C-factor of aromatic C–H stretching.

3- The pyrolysate distributions in Py–GC show that the molecular structure of isolated kerogen from the studied oil shales is characterized by a majorly organic sulphur (i.e., 2,3-dimethylthiophene) compound, along with

minor amounts of C_9 *n*-alkane and *o*-xylene compound, suggesting mainly high-sulphur Type II kerogen for potential of paraffinic oils with lower amount of wax.

4- Bulk kinetic analysis indicates that the kerogen Type II-S can be converted into high-sulphur oil over low geological temperatures range from 100 to 106 °C, agreeing to low Ro values in the range of 0.55–0.60%.

5- The highlighted results in this work suggest that substantial unconventional oil exploration operations from oil shale can be endorsed in the shallow deposits of the MCM Formation in the Lajjun Sub-basin, Western Central Jordan.

Data availability

All data generated or analysed during this study are included in this published article.

References

1. van Krevelen, D. W. *Coal: Typology, Chemistry, Physics, Constitution* Vol. 36, 173 (Elsevier, 1961).
2. Lille, U., Heinmaa, I. & Pehk, T. Molecular model of Estonian Kukersite kerogen evaluated by ^{13}C MAS NMR spectra. *Fuel* **82**, 799–804 (2003).
3. Wilkins, R. W. T. & George, S. C. Coal as a source rock for oil: A review. *Int. J. Coal Geol.* **50**, 317–361 (2002).
4. Pan, S. *et al.* Molecular structure and electronic properties of oil Shale Kerogen: An experimental and molecular modeling study. *Energy Fuels* **32**, 12394–12404 (2018).
5. Trewhella, M. J., Poplett, I. J. F. & Grint, A. Structure of Green River oil shale kerogen: Determination using solid state ^{13}C NMR spectroscopy. *Fuel* **65**, 541–546 (1986).
6. Eglinton, T. I., Larter, S. R. & Boon, J. J. Characterisation of kerogens, coals and asphaltenes by quantitative pyrolysis—Mass spectrometry. *J. Anal. Appl. Pyrolysis* **20**, 25–45 (1991).
7. Wiltfong, R. *et al.* Sulfur speciation in different kerogens by XANES spectroscopy. *Energy Fuels* **19**, 1971–1976 (2005).
8. Kelemen, S. R. *et al.* Direct characterization of kerogen by X-ray and solid-state ^{13}C nuclear magnetic resonance methods. *Energy Fuels* **21**, 1548–1561 (2007).
9. Hillier, J. L., Fletcher, T. H., Solum, M. S. & Pugmire, R. J. Characterization of macromolecular structure of pyrolysis products from a Colorado Green River oil shale. *Ind. Eng. Chem. Res.* **52**, 15522–15532 (2013).
10. Yan, J. W., Jiang, X. M., Han, X. X. & Liu, J. G. A. TG-FTIR investigation to the catalytic effect of mineral matrix in oil shale on the pyrolysis and combustion of kerogen. *Fuel* **104**, 307–317 (2013).
11. Fletcher, T. H. *et al.* Characterization of macromolecular structure elements from a Green River oil shale. II. Characterization of pyrolysis products by ^{13}C NMR, GC/MS, and FTIR. *Energy Fuels* **28**, 2959–2970 (2014).
12. Zheng, M. *et al.* Pyrolysis of Liulin coal simulated by GPU-based ReaxFFMD with cheminformatics analysis. *Energy Fuels* **28**, 522–534 (2014).
13. Huang, Y., Han, X. & Jiang, X. Characterization of Dachengzi oil shale fast pyrolysis by curie-point pyrolysis-GC-MS. *Oil Shale* **32**, 134–150 (2015).
14. Li, S. H., Ma, X. Q., Liu, G. C. & Guo, M. X. A. TG–FTIR investigation to the co-pyrolysis of oil shale with coal. *J. Anal. Appl. Pyrolysis* **120**, 540–548 (2016).
15. Alali, J., 2006. Recent Trends in Oil Shale. International Conference on Oils Shale. (Amman, Jordan).
16. Dyni, J.R. *Geology and Resources of Some World of Oil Shale Deposits*. Geological Survey, 42 (2006)
17. Alqudah, M., Ali, H. M., Van den Boorn, S., Podlaha, O. G. & Mutterlose, J. Calcareous nannofossils biostratigraphy of oil shales from Jordan. *GeoArabia* **19**(1), 117–140 (2014).
18. Ali, H. M. *Sedimentology of Cretaceous–Paleogene oil shales from Jordan* (Ruhr Universitat Bochum, 2013).
19. Shawabkeh, K. *Geological Map of Adir. Geological Map Division* (Natural Resources Authority, 1990).
20. Alqudah, M. *et al.* Eocene oil shales from Jordan-paleoenvironmental implications from reworked microfossils. *Mar. Pet. Geol.* **52**, 93–106 (2014).
21. Ali, H. M. *et al.* Ichnofabrics of Eocene oil shales from central Jordan and their use for paleoenvironmental reconstructions. *GeoArabia* **19**, 145–160 (2014).
22. Ali, H. M., Alqudah, M., Blessenohl, M., Podlaha, O. G. & Mutterlose, J. Depositional environment of Late Cretaceous to Eocene organic-rich marls from Jordan. *GeoArabia* **20**, 191–210 (2015).
23. Abed, A. M., Arouri, K. R. & Boreham, C. J. Source rock potential of the phosphorite–bituminous chalk–marl sequence in Jordan. *Mar. Pet. Geol.* **22**, 413–425 (2005).
24. El-Hasan, T. Geochemistry of redox-sensitive trace elements and its implication on the mode of formation of the Upper Cretaceous oil shales, Central Jordan. *N. Jb. Geol. Paläont. Abh.* **249**(3), 333–344 (2008).
25. Jaber, J., Abu-Rahmeh, T., Alawin, A. & Al-Kloub, N. Surface retorting of Jordanian oil shale and associated CO_2 emissions. *Jordan J. Mech. Ind. Eng.* **4**, 591–596 (2010).
26. Hakimi, M. H., Abdullah, W. H., Alqudah, M., Makeen, Y. & Mustapha, K. A. Organic geochemical and petrographic characteristics of the oil shales in the Lajjun area, Central Jordan: Origin of organic matter input and preservation conditions. *Fuel* **181**, 34–45 (2016).
27. Bender, F. *Geology of the Arabian Peninsula-Jordan. United States Geological Survey Professional Paper 560-I*, 36 (1975)
28. Camoin, G. *et al.* Late Maastrichtian, (69.5–65 Ma). In *Atlas of Tethys Palaeoenvironmental Maps. Explanatory Notes* (eds Dercourt, J. *et al.*) 179–196 (Gauthier-Villars, Paris, 1993).
29. Ziegler, M. Late Permian to Holocene paleofacies evolution of the Arabian Plate and its hydrocarbon occurrences. *GeoArabia* **6**, 445–504 (2001).
30. Alsharhan, A. S. & Nairn, A. E. M. *Sedimentary Basins and Petroleum Geology of the Middle East* 843 (Elsevier, 1997).
31. Powell, J. H. & Moh'd, B. K. Evolution of cretaceous to eocene alluvial and carbonate platform sequences in central and south Jordan. *GeoArabia* **16**, 29–82 (2011).
32. Alqudah, M., Hussein, M. A., van den Boorn, S., Podlaha, O. G. & Mutterlose, J. Biostratigraphy and depositional setting of Maastrichtian—Eocene oil shales from Jordan. *Mar. Pet. Geolo.* **60**, 87–104 (2015).
33. Yassini, I. Maastrichtian-lower eocene biostratigraphy and the planktonic foraminiferal biozonation in Jordan. *Rev. Esp. Micropaleontol.* **11**, 5–57 (1979).
34. Smadi, A. Cretaceous-paleogene biostratigraphy successions in Jordan. *Dirasat, pure science* **30**, 262–282 (2003).
35. Alqudah, M. *et al.* Impact of thermal maturation of the upper cretaceous bituminous limestone of attarat um ghudran central jordan on calcareous nannofossil preservation. *ACS Omega* **8**(42), 39830–39846. https://doi.org/10.1021/acsomega.3c06033 (2023).

36. Abd El-Motaal, E. & Kusky, T. Tectonic evolution of the intraplate s-shaped Syrian Arc Fold-Thrust Belt of the Middle East region in the context of plate tectonics, in *The Third International Conference of the Geology of Africa* vol. 2, 139–157 (2003)

37. Powell, J. Stratigraphy and sedimentation of the Phanerozoic rocks in central and south Jordan, in *Geological Mapping Division. Bulletin 11. Geological Directorate, Natural Resources Authority, Amman* (eds Part B: Kurnub, A., & Belqa Group) (1989

38. Yang, S. & Horsfield, B. Critical review of the uncertainty of Tmax in revealing the thermal maturity of orgnic matter in sedimentary rocks. *Int. J. Coal Geol.* **225**, 103500 (2020).

39. Taylor, G. H. *et al. Organic Petrology* (Gebrüder Borntraeger, 1998).

40. Weiss, H.M., Wilhelms, A. & Mills, N. *NIGOGA—The Norwegian Industry Guide to Organic Geochemical Analyses.* Edition 4.0. Accessed 16 November 2021; https://www.npd.no/globalassets/1-npd/regelverk/rapportering/bronner/eng/guide-organic-geochemical-analyses.pdf (2000)

41. Horsfield, B. Practical criteria for classifying kerogens: some observations from pyrolysis-gas chromatography. *Geochim. Cosmochim. Acta* **53**, 891–901 (1989).

42. Ganz, H. H. & Kalkreuth, W. IR classification of kerogen type, thermal maturation, hydrocarbon potential and lithological characteristics. *J. Southeast Asian Earth Sci.* **5**, 19–28 (1991).

43. Mastalerz, M., Hower, J. C. & Taulbee, D. N. Variations in chemistry of macerals as reflected by micro-scale analysis of a Spanish coal. *Geol. Acta* **11**, 483–493 (2013).

44. Ganz, H. & Kalkreuth, W. Application of infrared spectroscopy to the classification of kerogen-types and the evaluation of source rock and oil shale potentials. *Fuel* **66**, 708–711 (1987).

45. Wang, S., Tang, Y. & Schobert, H. H. FTIR and simultaneous TG/MS/FTIR study of Late Permian coals from Southern China. *J. Anal. Appl. Pyrolysis* **100**, 75–80 (2013).

46. Patricia, G. R. O., Blandón, A., Perea, C. & Mastalerz, M. Petrographic characterization, variations in chemistry, and paleoenvironmental interpretation of Colombian coals. *Int. J. Coal Geol.* **227**, 103516 (2020).

47. Burnham, A. K., Braun, R. L., Gregg, H. R. & Samoun, A. M. Comparison of methods for measuring kerogen pyrolysis rates and fitting kinetic parameters. *Energy Fuels* **1**, 452–458 (1987).

48. Burnham, A. K., Braun, R. L. & Samoun, A. M. Further comparison of methods for measuring kerogen pyrolysis rates and fitting kinetic parameters. *Org. Geochem.* **13**, 839–845 (1988).

49. Behar, F., Vandenbroucke, M., Tang, Y., Marquis, F. & Espitalie, J. Thermal cracking of kerogen in open and closed systems: Determination of kinetic parameters and stoichiometric coefficients for oil and gas generation. *Org. Geochem.* **26**(5–6), 321–339. https://doi.org/10.1016/S0146-6380(97)00014-4 (1997).

50. Schenk, H. J., Horsfield, B., Kroos, B., Schaefer, R. G. & Schwochau, K. Kinetics of petroleum formation and cracking. In *Petroleum and Basin Evolution* (eds Welte, D. H. *et al.*) 231–269 (Springer, 1997).

51. Inan, S., Alp, U. F., İnan, T., Yalçın, M. N. & Mann, U. Relationship between organic matter, sulphur and phosphate contents in Upper Cretaceous marine carbonates (Karaboğaz Formation, SE Turkey): Implications for early oil generation. *J. Pet. Geol.* **33**(4), 319–338 (2010).

52. Tissot, B. P. & Welte, D. H. *Petroleum formation and occurrence* 699 (Springer, 1984).

53. Hakimi, M. H., Abdullah, W. H. & Shalaby, M. R. Geochemical and petrographic characterization of organic matter in the Upper Jurassic Madbi shale succession (Masila Basin, Yemen): Origin, type and preservation. *Org. Geochem.* **49**, 18–29 (2012).

54. Pickel, W. *et al.* Classification of liptinite—ICCP System 1994. *Int. J. Coal Geol.* **169**, 40–61 (2017).

55. Sawada, K. & Akiyama, M. Carbon isotope composition of macerals separated from various kerogens by density separation method. *J. Jap. Assoc. Petrol. Technol.* **59**, 244–255 (1994).

56. Larter, S. R. & Douglas, A. G. A pyrolysis-gas chromatographic method for kerogen typing. *Phys. Chem. Earth* **12**, 579–583 (1980).

57. Dembicki, H. Jr., Horsfield, B. & Ho, T. T. Source rock evaluation by pyrolysis-gas chromatography. *AAPG Bull.* **67**(7), 1094–1103 (1983).

58. Jones, D. M., Douglas, A. G. & Connan, J. Hydrocarbon distributions in crude oil asphaltene pyrolyzates. 1. Aliphatic compounds. *Energy Fuels* **1**, 468–476 (1987).

59. Eglinton, T. I., Sinninghe Damste, J. S., Kohnen, M. E. L. & de Leeuw, J. W. Rapid estimation of the organic sulphur content of kerogens, coals and asphaltenes by pyrolysis-gas chromatography. *Fuel* **69**, 1394–1404 (1990).

60. Lehne, E. & Dieckmann, V. The significance of kinetic parameters and structural markers in source rock asphaltenes, reservoir asphaltenes and related source rock kerogens, the duvernay formation (WCSB). *Fuel* **86**, 887–901 (2007).

61. Makeen, Y. M., Abdullah, W. H. & Hakimi, M. H. Source rock characteristics of the Lower Cretaceous Abu Gabra Formation in the Muglad Basin, Sudan, and its relevance to oil generation studies. *Mar. Pet. Geol.* **59**, 505–516 (2015).

62. Dembicki, H. Three common source rock evaluation errors made by geologists during prospect or play appraisals. *AAPG Bull.* **93**, 341–356 (2009).

63. Petersen, H. I. Oil generation from coal source rocks: The influence of depositional conditions and stratigraphic age. *Geol, Surv. Denmark Greenl. Bull.* **7**, 9–12 (2005).

64. Hunt, J. M. Generation of gas and oil from coal and other terrestrial organic matter. *Org. Geochem.* **17**, 673–680 (1991).

65. Erik, N. Y. Hydrocarbon generation potential and miocene–pliocene paleoenvironments of the Kangal Basin (Central Anatolia, Turkey). *J. Asian Earth Sci.* **42**, 1146–1162 (2011).

66. Berner, R. A. & Raiswell, R. Burial of organic carbon and pyrite sulfur in sediments over Phanerozoic time: A new theory. *Geochim. Cosmochim. Acta* **47**, 855–862 (1983).

67. Dembicki, H. Three common source rock evaluation errors made by geologists during prospect or play appraisals. *Am. Assoc. Pet. Geol. Bull.* **93**, 341–356 (2009).

68. Chen, Z., Liu, X. & Jiang, C. Quick evaluation of source rock kerogen kinetics using hydrocarbon pyrograms from regular Rock-Eval analysis. *Energy Fuels* **31**, 1832–1841 (2017).

69. Behar, F. & Vandenbroucke, M. Chemical modeling of kerogens. *Org. Geochem.* **11**, 15–24 (1987).

70. Schaefer, R. G., Schenk, H. J., Hardelauf, H. & Harms, R. Determination of gross kinetic parameters for petroleum formation from Jurassic source rocks of different maturity levels by means of laboratory experiments. *Org. Geochem.* **16**, 115–120 (1990).

71. Hakimi, M. H., Abdullah, W. H., Mustapha, K. A. & Makeen, Y. M. Oil-generation characteristics of Mesozoic syn-rift Madbi source rock in the Masila Basin, Eastern Yemen: New insights from kerogen pyrolysis and bulk kinetic modelling. *Mar. Petrol. Geol.* **59**, 336–347 (2015).

72. Baskin, D. K. & Peters, K. E. Early generation and characteristics of a sulfur-rich Monterey kerogen. *Am. Assoc. Petroleum Geol. Bull.* **76**, 1–13 (1992).

73. Hakimi, M. H. *et al.* Pyrolysis analyses and bulk kinetic models of the Late Cretaceous oil shales in Jordan and their implications for early mature sulphur-rich oil generation potential. *Marine Pet. Geol.* **91**, 764–775 (2018).

74. Smith, G. C. & Cook, A. C. Petroleum occurrence in the Gippsland Basin and its relationship to rank and organic matter type. *Aust. Pet. Explor. Assoc. J.* **24**, 196–216 (1984).

Acknowledgements

Author contributions

M.H.H., M.A., K.A.M., A.K., M.A.L., A.R., M.A.V., D.K.N., take part in data analysis and interpretation, wrote the main manuscript text, results and discussions, and funding the work. A.A.A., S.A.A., take part in reviewing the manuscript.

Competing interests

The authors declare no competing interests.

Additional information

Correspondence and requests for materials should be addressed to M.H.H.

Reprints and permissions information is available at www.nature.com/reprints.

Publisher's note Springer Nature remains neutral with regard to jurisdictional claims in published maps and institutional affiliations.